Published in final edited form as:
Mol Cell. 2014 June 5; 54(5): 791–804. doi:10.1016/j.molcel.2014.03.047.

The 3M complex maintains microtubule and genome integrity

Jun Yan[1], **Feng Yan**[1], **Zhijun Li**[1], **Becky Sinnott**[4], **Kathryn M. Cappell**[4,7], **Yanbao Yu**[2], **Jinyao Mo**[5], **Joseph A. Duncan**[1,5], **Xian Chen**[2], **Valerie Cormier-Daire**[6], **Angelique W. Whitehurst**[4,8], and **Yue Xiong**[1,2,3,*]

[1]Lineberger Comprehensive Cancer Center, University of North Carolina at Chapel Hill, Chapel Hill, NC 27599-7295, USA.

[2]Department of Biochemistry and Biophysics, University of North Carolina at Chapel Hill, Chapel Hill, NC 27599-7295, USA.

[3]Program in Molecular Biology and Biotechnology, University of North Carolina at Chapel Hill, Chapel Hill, NC 27599-7295, USA.

[4]Department of Pharmacology, University of North Carolina at Chapel Hill, Chapel Hill, NC 27599-7295, USA.

[5]Department of Medicine, University of North Carolina at Chapel Hill, Chapel Hill, NC 27599-7295, USA.

[6]University Paris Descartes, Department of Genetics and INSERM U781, Hospital Necker Enfants-Malades, Paris, France

SUMMARY

CUL7, *OBSL1*, and *CCDC8* genes are mutated in a mutually exclusive manner in 3M and other growth retardation syndromes. The mechanism underlying the function of the three 3M genes in development is not known. We found that OBSL1 and CCDC8 form a complex with CUL7 and regulate the level and centrosomal localization of CUL7, respectively. CUL7 depletion results in altered microtubule dynamics, prometaphase arrest, tetraploidy and mitotic cell death. These defects are recaptured in *CUL7* mutated 3M cells and can be rescued by wild-type, but not 3M patients-derived *CUL7* mutants. Depletion of either OBSL1 or CCDC8 results in similar defects and sensitizes cells to microtubule damage as loss of CUL7 function. Microtubule damage reduces the level of CCDC8 that is required for the centrosomal localization of CUL7. We propose that CUL7, OBSL1, and CCDC8 proteins form a 3M complex that functions in maintaining microtubule and genome integrity and normal development.

*Correspondence: yxiong@email.unc.edu.
[7]Present address: Department of Medicine, Stanford University, 300 Pasteur Drive, L154 Stanford, CA94305, USA.
[8]Present address: Simmons Comprehensive Cancer Center, UT-Southwestern Medical Center, 5323 Harry Hines Blvd, Dallas, TX 75390, USA.

INTRODUCTION

To maintain genomic stability, sister chromatids have to be accurately segregated into daughter cells through mitosis, a short but extremely dynamic phase of the cell cycle. At the beginning of mitosis, chromatids line up at the midzone of the mitotic spindle and are then pulled toward opposite poles, leading to generation of daughter cells with identical genetic material (Walczak et al., 2010). During anaphase, the mitotic spindle rearranges to form a central spindle, which will be compressed by the contractile ring to form the midbody, a complex multi-protein structure also crucial for cytokinesis control at telophase (Glotzer, 2009). Cytokinesis failure leads to cell death or causes tetraploidy, believed to induce aneuploidy and contribute to tumorigenesis (Ganem et al., 2007).

Microtubules are a critical component of both mitosis and cytokinesis by forming the structure of both the mitotic and central spindles. Microtubules are cylindrical polymers made of α/β tubulin dimers that are dynamically unstable, making rapid switches between growth and shrinkage (Kline-Smith and Walczak, 2004; Kueh and Mitchison, 2009). They thereby guide chromatid alignment at prometaphase and segregation at anaphase and facilitate cleavage furrow ingression and abscission (Biggins and Walczak, 2003; Somers and Saint, 2003; Steigemann and Gerlich, 2009). The orderly assembly and disassembly of the microtubules are tightly regulated by numerous microtubule-associated proteins (Compton, 2000; Gadde and Heald, 2004; Glotzer, 2009). Defects in microtubule dynamics impair various cellular events, most notably mitosis. Inappropriate microtubule dynamics inhibits the alignment of chromosomes on the metaphase plate, leading to the activation of the spindle assembly checkpoint pathway (SAC) to inhibit the anaphase promoting complex (APC), thereby stalling mitotic progression to avoid chromatid mis-segregation (Musacchio and Salmon, 2007).

CUL7 is a member of the cullin family of proteins that function as scaffold proteins for E3 ubiquitin ligases by binding to the small RING finger protein, ROC1 (also known as RBX1), and substrates or substrate recruiting factors. CUL7 (1698 residues for human protein) is a large cullin protein and contains multiple functional domains. CUL7 is relatively evolutionarily young, having emerged as a functional protein after the appearance of vertebrates (Marin, 2009), localizes predominantly in the cytoplasm and binds to p53 (Andrews et al., 2006; Nikolaev et al., 2003). Deletion of *Cul7* in mice leads to intrauterine growth retardation and perinatal death (Arai et al., 2003). Mutations in the human *CUL7* gene are associated with 3M syndrome, named after three French authors, Miller, McKusick and Malvaux, who first described this heritable dwarfism (Miller et al., 1975). 3M syndrome is a severe autosomal recessive disorder characterized by short stature (120 – 130 cm for adults), unusual triangle-shaped facial features with a broad forehead, and widespread skeletal abnormalities in the neck, chest, shoulder, upper and lower back, fingers and legs (Huber et al., 2009; Huber et al., 2005; Maksimova et al., 2007). In addition to the skeleton, 3M syndrome also affects other systems, including reducing quantities of male hormones and increasing the risk of developing bulges in blood vessels. There is currently no treatment for the disease. Besides *CUL7*, two additional genes, *OBSL1* and *CCDC8*, have been found to be mutated in 3M syndrome. These three genes are mutated in a mutually exclusive manner, with *CUL7* being the most frequently mutated (~65%), followed by *OBSL1* (~30%)

and *CCDC8* (~5%) (Hanson et al., 2011a; Huber et al., 2011). Most mutations in these three genes cause truncations or frameshifts, indicating a loss-of-function as the cause of the disease. The molecular and cellular mechanism underlying the function of *CUL7* in development and the cellular mechanism of 3M syndrome are not known. This study was directed at resolving these issues, which led to the discovery that these three 3M gene products form a complex that functions in maintaining microtubule and genome integrity.

RESULTS

CUL7 localizes to the mitotic apparatus and regulates mitosis

To gain insight into the function of CUL7, we knocked down CUL7 using two different siRNA oligonucleotides, siCUL7-A and siCUL7-B, in U2OS human osteosarcoma cells and verified CUL7 depletion by direct immunoblot (Figure 1A, right). We found that depletion of CUL7 by either siRNA resulted in severe defects, including substantially decreased cell number, an increase in elongated and interconnected cells with two (tetraploidy) or multiple nuclei (polyploidy), and reduced cell motility as seen from cell clustering (Figure 1A, left). As these phenotypes are often associated with defects in cell cycle control, we next evaluated subcellular localization of CUL7 protein and found that a portion of CUL7 was readily detected on the centrosome and that the centrosomal localization of CUL7 persists throughout the cell cycle (Figure 1B). This finding suggested a potential function of CUL7 in mitosis and/or cytokinesis control.

To test this notion, we depleted CUL7 using siRNA and stained cells with an antibody specific to Ser10-phosphorylated histone H3, which correlates with chromosome condensation. We found that depletion of CUL7 had little effect on DNA condensation or decondensation (Figures S1A and S1B). However, when mitotic cells at different stages were quantified, the percentage of prometaphase cells was significantly increased by more than 60%, from 28.4 ± 3.5% in cells transfected with scrambled siRNA to 46.0 ± 3.0% in CUL7 depleted cells ($p = 0.016$, Figure 1C and see also Figure 6 showing a prolonged prometaphase with CUL7 depleted cells). Furthermore, the percentage of the prometaphase cells with unaligned chromosomes was increased in CUL7 depleted cells by 4-fold, from 13.3% to 53.3% ($n = 60$) (Figure 1D). Knockdown of CUL7 caused a slight increase in anaphase cells with lagging chromosomes (Figure S1C), which seemed to be fixed at telophase and cytokinesis (Figure S1D). Together, these results indicated that CUL7 depletion delayed mitotic progression due to impaired chromosome congression at prometaphase and also causes defects in cytokinesis.

CUL7 depletion caused noticeable cytokinesis defects, including elongated daughter cells with a long intercellular bridge, daughter cell fusion (Figure 1A), and wide spread cell death. We performed time-lapse imaging analyses to further examine this. U2OS cells treated with scrambled siRNA completed cytokinesis within about 2 hours, as measured by the time from forming a clear midbody at telophase to becoming flattened and undergoing daughter cells separation (Figure 1E and Movie S1). While CUL7 depleted cells formed furrows normally, they displayed evident cleavage defects in which many daughter cells remained close together after their DNA were decondensed. Some cells attempted to separate, causing a long intercellular bridge. A fraction of cells attempted abscission for as long as 5 hours, and

then died, as assessed by cell blebbing and shrinkage (Figure 1F and Movies S2). Some interconnected cells even entered the next round of mitosis (Figure 1G and Movie S3). Taken together, these results demonstrate that CUL7 plays a critical function during both mitosis and cytokinesis.

CUL7 is essential for normal microtubule dynamics

To explore the cellular mechanism underlying the function of CUL7 in mitotic control, we determined the effect of CUL7 depletion on the dynamics of microtubule, a cellular structure whose integrity is critically important for both mitosis and cytokinesis. Compared to cells transfected with scrambled siRNA, CUL7 depleted cells showed a significantly altered microtubule network at interphase as determined by both immunostaining of α-tubulin and imaging of U2OS cells stably expressing α-tubulin fused with enhanced green fluorescent protein (EGFP-α-tubulin) (Figure 2A). γ-tubulin staining showed that CUL7 depletion did not alter localization of the microtubule organization center (MTOC) (Figure S2). To further examine microtubule growth, we expressed EGFP tagged End-binding protein 1 (EB1), a microtubule plus-end tracking protein (+TIP) which when fused with EGFP generates fluorescent comets from the centrosome and allows the measurement of nucleation and microtubule dynamics in living cells (Piehl et al., 2004; Tirnauer et al., 2004). We found that CUL7 depleted U2OS cells showed irregular EB1 trails compared to control cells (Movies S4 and S5, and Figure 2B), indicating a function of CUL7 in maintaining microtubule integrity. The velocity of microtubule plus-end movement was also measured by tracing the position of EGFP-EB1 in the movies, and it was found that CUL7 depletion significantly ?(p-value)? increased microtubule plus-end growth rate ($n > 30$) (Figure 2C). Misregulated microtubule dynamics caused by CUL7 depletion could affect microtubule-kinetochore attachments, leading to the defects in mitotis and cytokinesis.

3M derived mutations in *CUL7* disrupt its function in maintaining genome integrity

Germline mutations in the human *CUL7* gene were found in patients with 3M syndrome, Yakut short stature syndromes and gloomy face syndrome (Huber et al., 2005; Maksimova et al., 2007). To determine whether the development of 3M syndrome is linked to the function of CUL7 in mitosis and cytokinesis control, we examined the ability of three missense 3M mutants, P861S, H1464P, Q1469R, and one truncation mutant, E1594fs, that target the DOC1 or ROC1-binding domains of CUL7 (Figures 3A and3B), in rescuing the defects in mitotis and cytokinesis caused by CUL7 depletion. Efficient knockdown of endogenous CUL7 and ectopic expression of wild type and mutant CUL7 were verified by qRT-PCR and western blot, respectively (Figures S3A and S3B). Knockdown of CUL7 resulted in significant accumulation of tetraploid and polyploid cells from 3% in cells transfected with scrambled siRNA to 9% in cells transfected with siRNA against *CUL7* (Figure 3C). Ectopic expression of wild-type CUL7 effectively rescued the defects in CUL7 depleted cells, reducing the tetraploid/polyploid cells to 5.2%. In contrast, ectopic expression of none of the four 3M-derived CUL7 mutants were able to rescue the defects and instead caused an elevation in the percentage of tetraploid and polyploid cells from 12.6% to 14.6%, indicative of a dominant negative effect. Supporting this finding, ectopic expression of two non-3M mutants of CUL7, one containing a small deletion in the DOC1 domain ($CUL7^{mtDOC1}$, deleting residues 863 to 869) and one disrupting ROC1 binding

(CUL7$^{\Delta ROC1}$, deleting residues 1,472 to 1,477, Figure S3C), also failed to rescue the mitotic defects in CUL7 depleted cells and similar to that of 3M-derived mutants, exacerbated the tetraploidy defects to 13% and 14%, respectively (Figures 3C, S3D and S3E). Thus, both the DOC1 domain dependent processivity and binding with ROC1 were impaired in 3M patients and are vital for CUL7 function in regulating cell proliferation and faithful division.

To provide further evidence linking the function of CUL7 in suppressing 3M syndrome and its function in mitosis, we investigated skin fibroblasts from two 3M patients bearing V1484GfsX68 (3M-1) and R1445X (3M-2) mutations, respectively. These two lines of 3M fibroblast cells contained 8.8% and 6.4% of tetraploid cells (n > 500), respectively, which is significantly ?(p-value)? higher than the percentage of tetraploid cells found in either NHF-1 cells from a normal human foreskin fibroblast cell line at similar passage (2.4%), and WI-38 cells from a normal human lung fibroblast cell line with much higher passage (3.2%) (Figure 3D, left). Confirming this result, FACS analyses showed that these two lines of 3M fibroblasts contain 6.69% and 3.31% of polyploid cells, significantly ?(p-value)? (4.6- and 2.3-fold, respectively) higher than that seen in either NHF-1 (1.48%) or WI-38 cells (1.42%, Figure 3E, right). These results suggest that defects in mitotis and cytokinesis caused by the loss of CUL7 function may contribute to development of 3M syndrome.

The 3M gene products CUL7, OBSL1 and CCDC8 form a complex

Recently, mutually exclusive mutations in *OBSL1* and *CCDC8* were identified in 3M patients that do not carry *CUL7* mutations (Hanson et al., 2011b; Hanson et al., 2009; Huber et al., 2010). Obscurin-like 1 (OBSL1) is a large (1896 residues) and putative cytoskeletal adaptor protein (Geisler et al., 2007), while CCDC8 is a coiled-coil domain containing protein without clear functions (Morris et al., 2011). Importantly, the mutations in these three genes occurred in a mutually exclusively manner, strongly suggesting that OBSL1, CCDC8, and CUL7 work in the same pathway. We first examined the interaction between OBSL1 and CCDC8 with CUL7 in cells triply transfected with plasmids expressing these three proteins. Reciprocal IP-western analyses demonstrated that each protein could be readily detected in the other two immune complexes, indicating these three proteins co-exist in the same complex (Figure 4A) and supporting the notion that they function on the same pathway. OBSL1 can also associate with three other known CUL7-interacting proteins, p53 and CUL9 (Figure S4A) and ROC1 (Figure S4B), but only in the presence of CUL7. We then performed a gel-filtration experiment and found that endogenous CUL7, CCDC8, p53, and ROC1 partially co-eluted in at least two distinct fractions: one (fractions 24 – 25) is around 440 kDa and one (fraction 17) is much larger, around 758 kDa (Figure 4B, blotting OBSL1 was not possible due to the lack of a suitable antibody). To map the OBSL1 and CCDC8 binding regions in CUL7, full length and various truncation mutants of CUL7 were ectopically expressed in 293T cells and their bindings with endogenous CCDC8 and co-expressed OBSL1 were determined by IP-western analysis. We found that OBSL1 binds to the C-terminal of CUL7, while both the N- and C-terminal of CUL7 could interact with CCDC8 (Figure S4C). We next performed a subcellular fractionation assay to determine where 3M proteins interact in the cell. This experiment showed that OBSL1 interacts with CUL7 and CCDC8 mainly in the cytoplasm (Figure 4C). Finally, to determine if OBSL1 and CCDC8 are also localized to the centrosome like CUL7, centrosomes of U2OS cells

overexpressed with Myc-OBSL1 were isolated through two steps of ultracentrifugation. Notably, a portion of OBSL1 and CCDC8 was clearly identified on the centrosome (Figure 4D). Together, these assays demonstrate that three 3M proteins physically interact with each other and may assemble a potentially very large complex, which we refer to as the 3M complex (see Discussion), that could contain as many as four additional proteins, CUL9, p53 and ROC1, as well as FBXW8 (see below).

FBXW8 is in the 3M complex

FBXW8 (also known as FBX29, FBW6) is an F-box protein and the only reported putative adaptor protein thus far for CUL7. FBXW8 brings SKP1 to CUL7 and forms a potentially atypical SCF-like E3 complex (Dias et al., 2002). Disruption of *Fbxw8*, similar to that of *Cul7*, causes pre- and post-natal growth retardation and death of two-thirds of embryos *in utero* (Tsunematsu et al., 2006; Tsutsumi et al., 2008). In an attempt to search for potential substrates of CUL7 complexes, we performed a mass spectrometric analysis of an affinity-purified FBXW8 complexes derived from 293T cells. Although this analysis has not yielded an obvious substrate that is targeted by FBXW8 to the CUL7 E3 ligase, it has identified three known FBXW8-interacting proteins (CUL7, CUL1 and SKP1), and OBSL1 and CCDC8 that were not previously reported to interact with FBXW8 (Figure 4E). This finding suggests that FBXW8 is a part of the 3M complex.

We confirmed the FBXW8-CCDC8 and FBXW8-OBSL1 interactions by co-immunoprecipitation assay (Figures 4F and4G). We further characterized the interaction between OBSL1 and FBXW8 and found that deletion of the F-box in FBXW8 (ΔF, residues 119 to 161), which is required for binding with SKP1, moderately affected the binding of FBXW8 to OBSL1. Deletion of the first WD40 domain in FBXW8 (ΔWD1, residues 201 to 326), which is required for binding with CUL7, or a linker region (ΔL, residues 162 to 200) which is required for binding with both CUL1 and CUL7 (Tsunematsu et al., 2006), significantly compromised the binding with OBSL1 (Figure 4G). These binding assays are consistent with the idea that FBXW8-OBSL1 interaction is bridged by CUL7.

OBSL1 and CCDC8 are required for maintaining microtubule and genome integrity

The fact that mutation of *CUL7, OBSL1* and *CCDC8* genes occur in the same disease in a mutually exclusive manner and that their products form a complex suggests that they function in the same pathway. To test this notion, we first characterized several siRNA oligonucleotides against either *OBSL1* or *CCDC8* and identified two siRNAs targeting each gene that work efficiently as verified by either qRT-PCR (Figure S5A) or western (Figure 5A). We found that depletion of either gene induced tetraploid and polyploid cells (Figure 5A), from 2.3% in cells transfected with scrambled siRNA oligonucleotides to an average of 9.0% or 11.6% in cells depleted for OBSL1 or CCDC8, respectively, slightly more severe than that in cells depleted for CUL7 (8.2%, Figure 5B). This result provides a piece of evidence that these three 3M proteins function in maintaining genome integrity.

To study whether OBSL1 or CCDC8 depletion also affects microtubule dynamics, U2OS cells depleted for OBSL1 or CCDC8 were treated with nocodazole for 2 hours to depolymerize microtubules, followed by a washout to allow for microtubule regrowth. Cells

depleted for OBSL1, like those depleted for CUL7, recovered their microtubules from nocodazole treatment more quickly than control cells transfected with scrambled siRNA as assayed by the overall microtubule fiber intensity (Figures 5C). Likewise, cells depleted for CCDC8 also recovered microtubules from nocodazole toxicity more quickly than control cells both in interphase (Figure 5D, upper panels) and during mitosis (Figure 5D, lower panels).

To further demonstrate the function of OBSL1 and CCDC8 in the regulation of microtubule dynamics, we knocked down the genes for both proteins in U2OS cells stably expressing EGFP-α-tubulin and found significant alterations of the microtubule network at interphase to a similar extent as seen in CUL7-depleted cells (Figure 5E). Importantly, double knock down of CUL7 with either OBSL1 or CCDC8 or triple depletion of all three 3M genes did not result in a significant further aggravation of the microtubule defects (Figure 5E, knocking down efficiency was verified in Figures S5B and S5C). Taken together, these results indicate that the three 3M genes, *CUL7*, *OBSL1* and *CCDC8*, share a function in the negative regulation of microtubule dynamics and the maintenance of genome integrity, and that they most likely act on the same pathway.

Loss of 3M gene function sensitizes cells to microtubule damage

To further investigate the function of CUL7, OBSL1, and CCDC8 in mitotic regulation, we depleted these proteins in a human lung tumor cell line (NCI-H1155) stably expressing histone H2B fused with EGFP (H2B-EGFP), which allows for the monitoring of chromosome dynamics and nuclear morphology in real-time throughout the cell cycle (Kavallaris, 2010). Cells were exposed to an otherwise innocuous dose of paclitaxel/taxol (10 nM), an anti-tumor agent that stabilizes microtubules and interferes with the alignment of chromosomes on the metaphase plate. Cells were monitored by live cell time-lapse imaging video microscopy and chromosome alignment was assessed by measuring the time between nuclear envelope breakdown and the onset of anaphase. Depletion of either CUL7 or OBSL1 dramatically delayed mitotic transit time. While control cells transfected with scrambled siRNA spent an average of 96.9 minutes between prometaphase and metaphase, this process took 442 minutes and 417 minutes in cells transfected with siRNA against *CUL7* or *OBSL1*, respectively (Figure 6A, upper panel and Figure S6A). In cells treated with low dose taxol (10 nM), both CUL7 and OBSL1 depletion greatly delayed chromosome alignment and increased the transit time between prometaphase and metaphase from an average of 194 minutes in cells transfected with scrambled siRNA oligos to 969 minutes and 707 minutes, respectively (Figure 6A, lower panel). Most of these cells went through mitosis erroneously, exiting as dead cells, as a single cell, as cells divided into more than two cells, or as multinucleated cells (Figure 6B). Consistent with these results, CUL7 or OBSL1 depletion induces mono- and multi-polar mitotic spindles, an effect that is further enhanced by 1 nM taxol treatment (Figure 6C). Co-depletion of MAD2 completely rescued siCUL7 or siOBSL1 induced prometaphase delay (Figure 6D and Figure S6C, D), suggesting that CUL7 or OBSL1 depletion activated the spindle activation checkpoint (SAC). Surprisingly, depletion of CCDC8 did not generate noticeable phenotypes (Figure S6B). Further study demonstrated that *CCDC8* was expressed at a barely detectable level in NCI-H1155 cells (Figure S6D), which suggests that *CCDC8* may be silenced in these cells and could explain

why the cells were not responsive to siCCDC8. Together, these results demonstrate similar functions of *CUL7*, *OBSL1*, and *CCDC8* in controlling prometaphase and indicate that the mitotic defects induced by CUL7, OBSL1, or CCDC8 depletion are mediated through a loss of microtubule integrity.

CCDC8 is required for centrosomal localization of CUL7

To provide further evidence for the functional interaction among 3M proteins, we investigated the regulatory relationship among them with a focus on *CUL7*, the only enzyme-encoding and most frequently mutated gene of the three. Depletion of OBSL1 did not seem to significantly affect the levels of CCDC8 expression (data not shown), nor did depletion of CCDC8 affect the levels of CUL7 expression (Figure 5A). There are, however, two significant impacts on CUL7 upon losing either OBSL1 or CCDC8 function. First, depletion of OBSL1 in NCI-H1155 cells and U2OS cells substantially reduced the steady state levels of both *CUL7* mRNA and protein (Figures S6A, S7A). This is consistent with a previous report showing that in a different cell line, HEK293, knocking down *OBSL1* reduced both *CUL7* mRNA and protein (Hanson et al., 2009). Second, silencing *CCDC8*, which did not affect levels of CUL7 expression (Figure 5A), significantly ?(p-value)? compromised the centrosomal localization of CUL7 in both interphase and mitotic cells (Figure 7A and S7B). These results suggest that the function of CUL7 is subject to regulation by the other two 3M proteins, specifically at the level of expression by OBSL1 and centrosomal localization by CCDC8.

Microtubule damage reduces CCDC8 expression and diminishes the centrosomal localization of CUL7

To further substantiate the regulation of CUL7 by the other 3M proteins, we focused on the regulation of CUL7 by CCDC8 and examined the impacts of microtubule damage on this regulation. Treatment of U2OS cells with either nocodazole or taxol had no significant ?(p-value)? effect on the level of CUL7 expression, but substantially reduced the levels of CCDC8 expression (Figure 7B). In accordance with CCDC8 reduction, both nocodazole and taxol treatments diminished centrosomal localization of CUL7 (Figures 7C, S7C). Time course experiments demonstrated that CCDC8 reduction following microtubule damage was not an acute effect but instead took more than 8 hours (Figure 7D), which correlated closely with the loss of centrosomal localization of CUL7 (Figures 7E and S7D). To determine whether the reduction of CCDC8 and diminished centrosomal localization of CUL7 are caused by microtubule damage or the cell cycle arrest at mitosis, we synchronized NHF-1 cells at different phases and verified the synchrony by FACS analysis (Figure S7E). Direct immunoblotting analyses demonstrated that the steady state levels of both CUL7 and CCDC8, as well as CUL9, remain relatively constant throughout the cell cycle (Figure 7F and quantification in Figure S7F). Treatment of microtubule-damaged cells with a proteasome inhibitor did not restore the levels of CCDC8 expression (Figure S7G). Instead, quantitative PCR analysis demonstrated that *CCDC8* mRNA was reduced by microtubule damage (Figure S7H), suggesting that transcriptional inhibition is a major mechanism for microtubule damage-induced CCDC8 reduction. While the CCDC8 protein is reduced by nearly 70% 24 hours after microtubule damage, *CCDC8* mRNA was only reduced by about 40%, suggesting an additional posttranscriptional mechanism in the regulation of CCDC8

level after microtubule damage. Taking these results together, we demonstrated that microtubule damages affect the function of CUL7 protein, in part, by down regulating the levels of CCDC8, which leads to the diminished centrosomal localization of CUL7.

DISCUSSION

A cellular mechanism for 3M syndrome and other developmental disorders

In addition to 3M syndrome, *CUL7* and *OBSL1* mutations were also found in Yakuts syndrome, le Merrer syndrome (also known as loomy face syndrome) and Silver-Russel syndromes (SRS) (Akawi et al., 2011; Huber et al., 2005; Maksimova et al., 2007), expanding the scope of 3M syndrome and linking these rare and different primordial growth disorders into a potentially single disease with a common underlying molecular and cellular mechanism. Three lines of evidence reported in this paper led us to propose a mechanism—regulation of microtubule dynamics and maintenance of genome integrity—whose disruption underlies the development of 3M syndrome and other related primordial growth disorders. First, consistent with their mutually exclusive mutation patterns, three 3M proteins, CUL7, OBSL1 and CCDC8, physically interact with each other and form a joint complex. Deletion or knockdown of each individual 3M gene resulted in very similar microtubule, mitotic and cytokinesis defects. Combined depletion of two or three 3M genes did not synergistically cause any additive effect. Second, fibroblasts derived from *CUL7*-mutated 3M patients exhibit similar mitotic defects and polyploidy that can be rescued by the ectopic expression of wild-type, but not mutant *CUL7*. Third, among the 3M proteins, CUL7, is functionally regulated by the other two, OBSL1 and CCDC8, supporting the notion that the functions of these three genes are integrated into a single biochemical complex and cellular pathway. Affecting such a fundamental cellular process as controlling microtubule and genome integrity that is essential to virtually all cells, explains the wide spread abnormalities in many different cell types and body systems seen in 3M patients.

We therefore suggest that there exists *in vivo* a distinct protein complex, which we refer to as the 3M complex, whose functional impairment leads to severe defects in microtubule dynamics, chromosome segregation, cell survival and organismal growth.

The 3M complex

We have demonstrated in this study that three 3M proteins, CUL7, OBSL1 and CCDC8, form an integral complex. Given their mutually exclusive mutation pattern, the nearly complete coverage of 3M syndrome by their combined mutations and the functional regulation of CUL7 by OBSL1 and CCDC8, we postulate that CUL7, OBSL1 and CCDC8 constitute the core 3M complex. Besides CUL7, OBSL1 and CCDC8, the 3M complex likely interacts with multiple additional proteins, including notably ROC1—the presumptive catalytic RING figure protein, FBXW8—a potential substrate adapter, CUL9—a binding partner and downstream effector of CUL7, and p53—a checkpoint gene whose function has long been implicated in mitotic control. The exact biochemical function of each of these four, and possibly other, proteins interacting with 3M complex remains to be determined. Identification of the function of the 3M genes and complex in the regulation of microtubule dynamics offers a functional assay for elucidating the physiological significance of the

interaction between the 3M complex and these proteins. One such example is provided in the accompanying paper where we showed that CUL9 is a downstream effector of the 3M complex.

The 3M complex functions in maintaining microtubule integrity

We suggest that a critical function of the 3M complex is to regulate microtubule dynamics, for example, by controlling the level of a microtubule stabilizer. Previous studies have suggested a variety of different functions for the 3M proteins. These include a function of CUL7 in vascular morphogenesis (Arai et al., 2003) and targeting insulin growth factor for degradation (Xu et al., 2008), a function of OBSL1 in myocyte modeling (Geisler et al., 2007), in epithelial-mesenchymal transition of choriocarcinoma cells (Fu et al., 2010) and in Golgi morphology and dendrite patterning (Litterman et al., 2011). Four lines of evidence support the notion that the severe and broad defects seen in 3M patients and *Cul7* mutant mice can be better explained by an impaired function of the 3M complex in the regulation of microtubule dynamics.

First, loss of 3M proteins accelerates microtubule growth in both interphase and mitotic cells, implying a function for the 3M complex in either inhibiting microtubule growth or promoting microtubule catastrophe. Second, the loss of function of 3M complex proteins sensitizes cells to the treatment by low dose taxol, which binds to β tubulin in the microtubules and impairs GTP hydrolysis and the function of microtubules. Third, fibroblasts derived from 3M patients and cells depleted for individual 3M genes develop similar aneuploidy, and mitotic and cytokinesis defects, all of which can be caused by a defect in sensing or repairing microtubule damages. Fourth, we have identified one function of CCDC8 in localizing CUL7 to centrosome. Furthermore, we showed that treatment of cells with microtubule damaging agents reduces the cellular levels of CCDC8 and that this reduction is associated with the loss of centrosomal localization of CUL7. Collectively, these results not only established a function of 3M proteins and the 3M complex in maintaining microtubule integrity, but also the regulation of the 3M complex in response to microtubule damage.

Our study also raises a number of critical questions. How does microtubule damage regulate the expression of CCDC8 and thus the centrosomal localization of CUL7? How are the formation of the 3M complex and the association of other proteins with CUL7 regulated? What is the role of p53, which binds to, but is not degraded by, CUL7 in the 3M complex? The establishment of the cellular function of the 3M complex in maintaining microtubules and genome integrity should significantly facilitate the investigation of these and other questions important for the understanding of this newly discovered 3M complex in mitotic regulation and development.

EXPERIMENTAL PROCEDURES

Large-scale immunoprecipitation and mass spectrometry

To isolate and identify FBXW8-interacting proteins, retrovirus encoding FLAG-SBP-FBXW8 was generated and infected into HEK293T cells, followed by puromycin selection

to make a stable cell line. Two 150mm dishes of cells with around 90% confluence were collected, and proteins extracted with NP40 buffer. FBXW8 protein complexes were purified with streptavidin sepharose (GE) and eluted with 50 mM biotin (Sigma), followed by trypsin digestion and mass spectrometric analysis. For desalting and nano LC-ESI MS/MS, after digestion, the tryptic peptides were dried and redissolved into 200 μL 5% acetonitrile (ACN) and 0.5% trifluoroacetic acid (TFA). The peptides were cleaned using a desalting column (PepClean C18, Pierce) according to the manufacturer's protocol. A minor modification of the protocol was made to include larger elution volume (200 μL) and repeated three times in order to increase the peptide recovery. The elution solution was lyophilized and resuspended into buffer A (2% ACN, 98% water and 0.1% formic acid) prior to LCMS separation.

For nano-scale reversed-phase liquid chromatography electrospray ionization tandem mass spectrometry (RPLC-ESI MS/MS) analysis was performed on an Eksigent Ultra-LTQ Orbitrap Velos system (Thermo Scientific), approximately 3 μL samples were loaded onto an IntegraFrit column (C18, 75 μm×15 cm, 300 Å, 5 μm, New Objective). A linear gradient was run from 100% buffer A to 40% buffer B (98% acetonitrile, 2% water and 0.1% formic acid) for 100 minutes and then went to 80% B in another 10 minutes. The gradient stayed in 80% B for 5 minutes and went back to initial status in another 5 minutes. Eluted peptides were acquired data-dependently using XCalibur software (version 2.1, Thermo Scientific) with full ion scan mode over m/z range 300-2,000. The top five parent ions in each MS full scan were selected for further MS/MS analysis.

For database search, raw files acquired from LTQ Orbitrap were processed through Proteome Discoverer software (version 1.2, Thermo Scientific) and searched against UniProKB database (Release 2011_12, 20246 human sequences). Here, the human sequences were extracted from the complete database using Proteome Discoverer software with “HUMAN” keyword. Oxidation (M) was set as variable modification. Peptide and protein tolerance were set to 200 ppm and 0.8 Da, respectively. Only distinct proteins and peptides containing seven amino acids or longer were accepted in the final result. The decoy database search option was checked in order to get the approximate false-discovery-rate (FDR). Only peptide confidence with less than 1% FDR was included.

Gel Filtration

Cell lysates of 293T cells were fractionated using size exclusion chromatography. Lysates, 0.5 ml) were run on Superose 6 10/300 GL (GE Healthcare) using an AKTA Purifier (GE Healthcare) liquid chromotography system with a flow rate of 0.4 ml/min in buffer consisting of 50 mM Tris-HCl (pH 7.4), 1 mM EDTA, 0.1% CHAPS, 1mM DTT and 150 mM NaCl. Fractions were collected from 7.2 ml to 17.6 ml and analyzed by western blot analysis. The approximate molecular weight was calculated after calibration of the column with Gel Filtration Standards (Bio-Rad).

Centrosome Isolation

Lysates from U2OS cells transfected with myc-OBSL1 were first applied to 20% ficoll cushion and centrosomes were concentrated in the layer between cushion and lysates after

ultra-centrifugation. Then centrosomes were collected and applied to a discontinous sucrose gradient (40%, 50% and 70%). After ultra-centrifugation, gradient was collected from top to bottom, and samples were subject to WB analysis.

Cellular Fractionation

U2OS cells were collected and cell pellet washed with cold PBS, followed by resuspension in cold cytosol extraction (CE) buffer (50 mM Tris-HCl, pH 7.5, 100 mM NaCl, 200 nM sucrose, 0.05% Triton X-100n and 1 mM EGTA) plus protease inhibitor cocktails. Resuspended cells were incubated on ice for 10 min, followed by centrifugation with the supernatant containing cytosol proteins and the pellet the intact nuclei. The pellet was washed and then resuspended in CE buffer, and a portion was boiled to get total nuclear protein fraction (N). The remaining nuclear proteins were sonicated. Both the cytosol proteins and the sonicated nuclear proteins were centrifuged at top speed for 30 minutes to obtain the cytosol proteins (C) and nuclear soluble proteins (NS).

Cell Synchronization

Pre-synchronized NHF1 cells at G0 phase were obtained by forcing them to grow over-confluently for 2 days. The cells were re-plated, and then the cells were collected 8 hours after re-plating to get G1 cells. To get S, G2 and M phase cells, re-plated cells were treated with aphidicolin (2ug/ml). Twenty-four hours later, the drug was washed out and the cells were collected 3 hours post-release (S) or 8 hours post-release (G2). Colcemid (100ng/ml) was added 8 hours post-release of aphidicolin, and then cells were collected 4 hours later to obtain M phase cells.

Live-Cell Microscopy

U2OS cells stably expressing GFP-α-tubulin and GFP-ubiquitin were cultured in 35 mm glass bottom dishes (MatTeK), and transfected with scrambled or CUL7 siRNA. After 48 hours, live-cell microscopy was carried out on the BioStation system (Nikon). Images were obtained every 5 minutes for 16 hours. U2OS cells transiently expressed with GFP-EB1 were studied with living cells microscopy, and images were obtained every 5 seconds for a period of 3 minutes. Human lung cancer NCI-H1155 cells stably expressing GFP-Histone H2B were generated through infecting cells with pCLNCX-GFP-Histone H2B retrovirus. For imaging, the NCI-H1155-GFP-Histone H2B line was transfected with the indicated siRNA and plated in a 96-well format followed by carrier or paclitaxel treatment 48 hours post transfection. At 72 hours post-transfection, imaging began on a BD Pathway 855 bio-imager using a 20X objective. Images were collected at 14.5 minutes intervals for the next 42 hours. Image sequences were generated using ImageJ. Image sequences were then evaluated for the indicated parameters manually.

For statistical analysis, all P values were calculated with Student's t-test and $P<0.05$ was considered as significant.

Additional details and other experimental procedures used in this paper, including plasmids, siRNA and primer sequences, antibodies and immunological procedures, cell culture, transfection, and flow cytometry procedures are available in the Supplemental Information.

Supplementary Material

Refer to Web version on PubMed Central for supplementary material.

Acknowledgments

We are grateful to Ted Salmon, Jim Bear and Steve Rogers for the insightful discussions and assistance throughout this study, Sarah Jackson and Jordon Kardos for critically reading the manuscript. J.A.D. was supported by the Burroughs Wellcome Fund Career Award for Medical Scientists. This study was supported by NIH grants CA154699 to A.W.W. and CA068377 to Y.X.

REFERENCES

Akawi NA, Ali BR, Hamamy H, Al-Hadidy A, Al-Gazali L. Is autosomal recessive Silver-Russel syndrome a separate entity or is it part of the 3-M syndrome spectrum? Am. J. Med. Genet. 2011; A155A:1236–1245. [PubMed: 21548126]

Andrews P, He YJ, Xiong Y. Cytoplasmic localized ubiquitin ligase cullin 7 binds to p53 and promotes cell growth by antagonizing p53 function. Oncogene. 2006; 25:4534–4548. [PubMed: 16547496]

Arai T, Kasper JS, Skaar JR, Ali SH, Takahashi C, DeCaprio JA. Targeted disruption of p185/Cul7 gene results in abnormal vascular morphogenesis. Proc. Natl. Acad. Sci. U. S. A. 2003; 100:9855–9860. [PubMed: 12904573]

Biggins S, Walczak CE. Captivating capture: how microtubules attach to kinetochores. Curr. Biol. 2003; 13:R449–460. [PubMed: 12781157]

Compton DA. Spindle assembly in animal cells. Annu. Rev. Biochem. 2000; 69:95–114. [PubMed: 10966454]

Dias DC, Dolios G, Wang R, Pan ZQ. CUL7: A DOC domain-containing cullin selectively binds Skp1.Fbx29 to form an SCF-like complex. Proc Natl Acad Sci U S A. 2002; 99:16601–16606. [PubMed: 12481031]

Fu J, Lv X, Lin H, Wu L, Wang R, Zhou Z, Zhang B, Wang YL, Tsang BK, Zhu C, et al. Ubiquitin ligase cullin 7 induces epithelial-mesenchymal transition in human choriocarcinoma cells. J. Biol. Chem. 2010; 285:10870–10879. [PubMed: 20139075]

Gadde S, Heald R. Mechanisms and molecules of the mitotic spindle. Curr. Biol. 2004; 14:R797–805. [PubMed: 15380094]

Ganem NJ, Storchova Z, Pellman D. Tetraploidy, aneuploidy and cancer. Curr. Opin. Genet. Dev. 2007; 17:157–162. [PubMed: 17324569]

Geisler SB, Robinson D, Hauringa M, Raeker MO, Borisov AB, Westfall MV, Russell MW. Obscurin-like 1, OBSL1, is a novel cytoskeletal protein related to obscurin. Genomics. 2007; 89:521–531. [PubMed: 17289344]

Glotzer M. The 3Ms of central spindle assembly: microtubules, motors and MAPs. Nat. Rev. Mol. Cell Biol. 2009; 10:9–20. [PubMed: 19197328]

Hanson D, Murray PG, Black GC, Clayton PE. The genetics of 3-m syndrome: unravelling a potential new regulatory growth pathway. Horm Res Paediatr. 2011a; 76:369–378. [PubMed: 22156540]

Hanson D, Murray PG, O'Sullivan J, Urquhart J, Daly S, Bhaskar SS, Biesecker LG, Skae M, Smith C, Cole T, et al. Exome sequencing identifies CCDC8 mutations in 3-M syndrome, suggesting that CCDC8 contributes in a pathway with CUL7 and OBSL1 to control human growth. Am. J. Hum. Genet. 2011b; 89:148–153. [PubMed: 21737058]

Hanson D, Murray PG, Sud A, Temtamy SA, Aglan M, Superti-Furga A, Holder SE, Urquhart J, Hilton E, Manson FD, et al. The primordial growth disorder 3-M syndrome connects ubiquitination to the cytoskeletal adaptor OBSL1. Am. J. Hum. Genet. 2009; 84:801–806. [PubMed: 19481195]

Huber C, Delezoide AL, Guimiot F, Baumann C, Malan V, Le Merrer M, Da Silva DB, Bonneau D, Chatelain P, Chu C, et al. A large-scale mutation search reveals genetic heterogeneity in 3M syndrome. Eur. J. Hum. Genet. 2009; 17:395–400. [PubMed: 19225462]

Huber C, Dias-Santagata D, Glaser A, O'Sullivan J, Brauner R, Wu K, Xu X, Pearce K, Wang R, Uzielli ML, et al. Identification of mutations in CUL7 in 3-M syndrome. Nat. Genet. 2005; 37:1119–1124. [PubMed: 16142236]

Huber C, Fradin M, Edouard T, Le Merrer M, Alanay Y, Da Silva DB, David A, Hamamy H, van Hest L, Lund AM, et al. OBSL1 mutations in 3-M syndrome are associated with a modulation of IGFBP2 and IGFBP5 expression levels. Hum. Mutat. 2010; 31:20–26. [PubMed: 19877176]

Huber C, Munnich A, Cormier-Daire V. The 3M syndrome. Best Pract Res Clin Endocrinol Metab. 2011; 25:143–151. [PubMed: 21396581]

Kavallaris M. Microtubules and resistance to tubulin-binding agents. Nat Rev Cancer. 2010; 10:194–204. [PubMed: 20147901]

Kline-Smith SL, Walczak CE. Mitotic spindle assembly and chromosome segregation: refocusing on microtubule dynamics. Mol. Cell. 2004; 15:317–327. [PubMed: 15304213]

Kueh HY, Mitchison TJ. Structural plasticity in actin and tubulin polymer dynamics. Science. 2009; 325:960–963. [PubMed: 19696342]

Litterman N, Ikeuchi Y, Gallardo G, O'Connell BC, Sowa ME, Gygi SP, Harper JW, Bonni A. An OBSL1-Cul7Fbxw8 ubiquitin ligase signaling mechanism regulates Golgi morphology and dendrite patterning. PLoS Biol. 2011; 9:e1001060. [PubMed: 21572988]

Morris MR, Ricketts CJ, Gentle D, McRonald F, Carli N, Khalili H, Brown M, Kishida T, Yao M, Banks RE, et al. Genome-wide methylation analysis identifies epigenetically inactivated candidate tumour suppressor genes in renal cell carcinoma. Oncogene. 2011; 30:1390–1401. [PubMed: 21132003]

Maksimova N, Hara K, Miyashia A, Nikolaeva I, Shiga A, Nogovicina A, Sukhomyasova A, Argunov V, Shvedova A, Ikeuchi T, et al. Clinical, molecular and histopathological features of short stature syndrome with novel CUL7 mutation in Yakuts: new population isolate in Asia. J. Med. Genet. 2007; 44:772–778. [PubMed: 17675530]

Marin I. Diversification of the cullin family. BMC Evol Biol. 2009; 9:267. [PubMed: 19925652]

Miller JD, McKusick VA, Malvaux P, Temtamy S, Salinas C. The 3-M syndrome: a heritable low birthweight dwarfism. Birth Defects Orig Artic Ser. 1975; 11:39–47. [PubMed: 1218233]

Musacchio A, Salmon ED. The spindle-assembly checkpoint in space and time. Nat Rev Mol. Cell. Biol. 2007; 8:379–393. [PubMed: 17426725]

Neef R, Klein UR, Kopajtich R, Barr FA. Cooperation between mitotic kinesins controls the late stages of cytokinesis. Curr Biol. 2006; 16:301–307. [PubMed: 16461284]

Nikolaev AY, Li M, Puskas N, Qin J, Gu W. Parc: a cytoplasmic anchor for p53. Cell. 2003; 112:29–40. [PubMed: 12526791]

Piehl M, Tulu US, Wadsworth P, Cassimeris L. Centrosome maturation: measurement of microtubule nucleation throughout the cell cycle by using GFP-tagged EB1. Proc. Natl. Acad. Sci. U. S. A. 2004; 101:1584–1588. [PubMed: 14747658]

Somers WG, Saint R. A RhoGEF and Rho family GTPase-activating protein complex links the contractile ring to cortical microtubules at the onset of cytokinesis. Dev. Cell. 2003; 4:29–39. [PubMed: 12530961]

Steigemann P, Gerlich DW. Cytokinetic abscission: cellular dynamics at the midbody. Trends Cell Biol. 2009; 19:606–616. [PubMed: 19733077]

Tirnauer JS, Salmon ED, Mitchison TJ. Microtubule plus-end dynamics in Xenopus egg extract spindles. Mol. Biol. Cell. 2004; 15:1776–1784. [PubMed: 14767058]

Tsunematsu R, Nishiyama M, Kotoshiba S, Saiga T, Kamura T, Nakayama KI. Fbxw8 is essential for Cul1-Cul7 complex formation and for placental development. Molecular and cellular biology. 2006; 26:6157–6169. [PubMed: 16880526]

Tsutsumi T, Kuwabara H, Arai T, Xiao Y, Decaprio JA. Disruption of the Fbxw8 gene results in pre- and postnatal growth retardation in mice. Molecular and cellular biology. 2008; 28:743–751. [PubMed: 17998335]

Walczak CE, Cai S, Khodjakov A. Mechanisms of chromosome behaviour during mitosis. Nat. Rev. Mol. Cell. Biol. 2010; 11:91–102. [PubMed: 20068571]

Xu X, Sarikas A, Dias-Santagata DC, Dolios G, Lafontant PJ, Tsai SC, Zhu W, Nakajima H, Nakajima HO, Field LJ, et al. The CUL7 E3 ubiquitin ligase targets insulin receptor substrate 1 for ubiquitin-dependent degradation. Mol. Cell. 2008; 30:403–414. [PubMed: 18498745]

HIGHLIGHTS

- A novel and mammalian specific complex regulating microtubule and cell division
- A mechanism for 3M syndrome and related development disorders
- CCDC8 maintains centrosomal localization of CUL7 and is reduced by microtubule damage

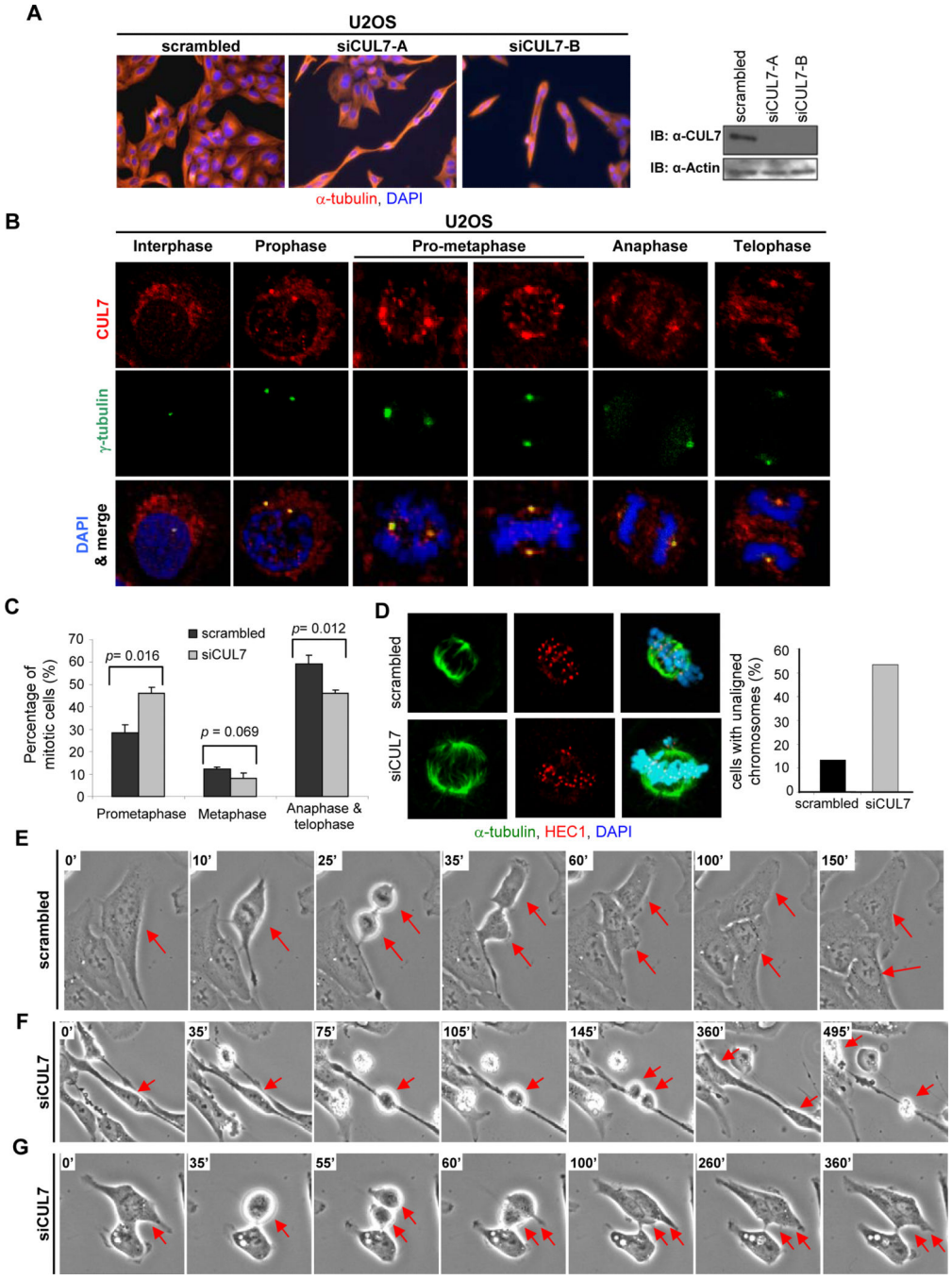

Figure 1. CUL7 protein localizes to mitotic apparatus and is functionally important for mitosis

(A) U2OS cells were transfected with the indicated siRNA for 3 days. Knockdown efficiency was verified by western blotting (right panel) and cells were stained with anti-α-tubulin antibody and DAPI.

(B) U2OS cells were stained with antibodies specific to CUL7, γ-tubulin and DAPI.

(C) U2OS cells transfected with scrambled siRNA or siRNA against CUL7 were stained with DAPI and mitotic cells (at least 100 cells for each sample) were examined microscopically. Percentage of cells in each phase was plotted. Bars represent mean of three

independent experiments, and error bars indicate standard deviation. P values indicate significant differences to control cells by t-test.

(D) Control or CUL7 depleted cells were stained with DAPI and antibodies to α-tubulin, and kinetochore protein HEC1. Prometaphase cells with obvious unaligned chromosomes were scored and plotted.

(E, F, G) U2OS cells were treated with scrambled or CUL7 siRNA for 48 hours. Cells were observed by time-lapse microscopy. The images are stills of the movies at the indicated time points. See also Movie S1-3.

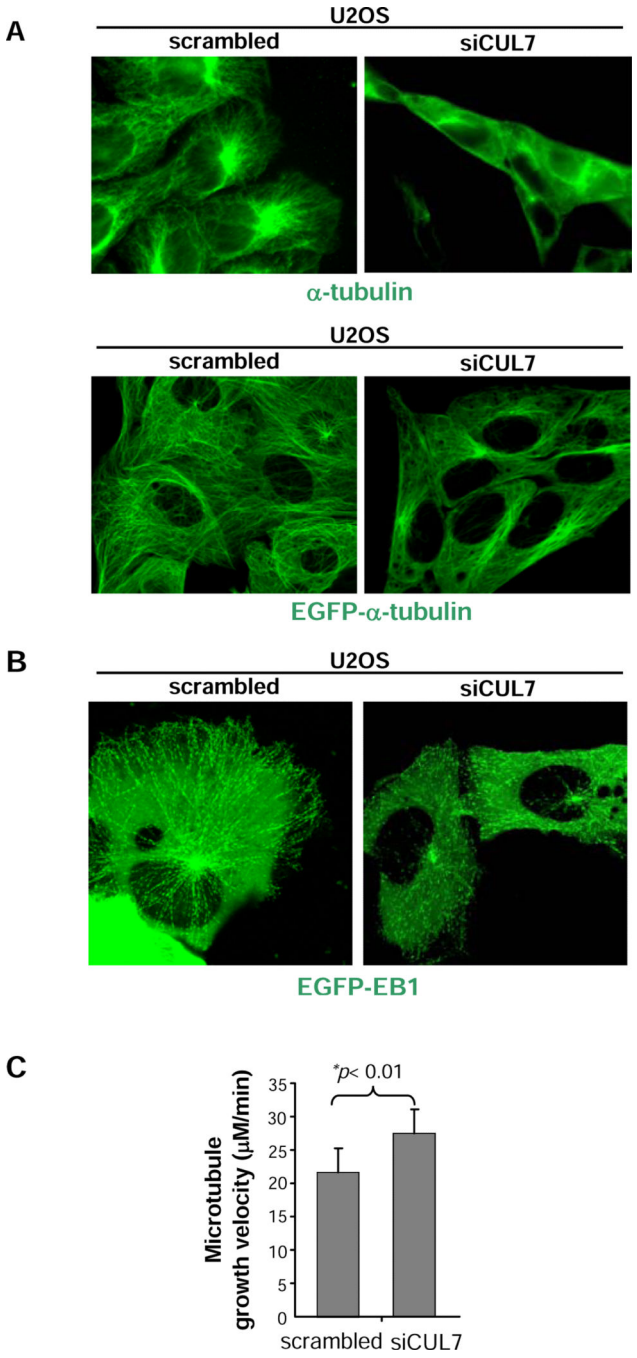

Figure 2. CUL7 regulates microtubule dynamics

(A) U2OS or U2OS/EGFP-α-tubulin cells were treated with scrambled or CUL7 siRNA (siCUL7-A) for 72 hours. Microtubule organization was visualized by α-tubulin staining or observing EGFP-α-tubulin in living cells with confocal microscopy. See also Figure S2. (B, C) U2OS cells were transfected with scrambled or CUL7 siRNA for 24 hours and then EGFP-EB1. Time-lapse microscopy was performed 24 hours after EGFP-EB1 transfection. The images represent overlay of twenty consecutive pictures showing microtubules growth path (B). See also Movie S4, 5. (C) The growing velocity of individual microtubules was

measured. Error bars indicate standard deviation (n>30). P values indicate significant differences to control cells by t-test.

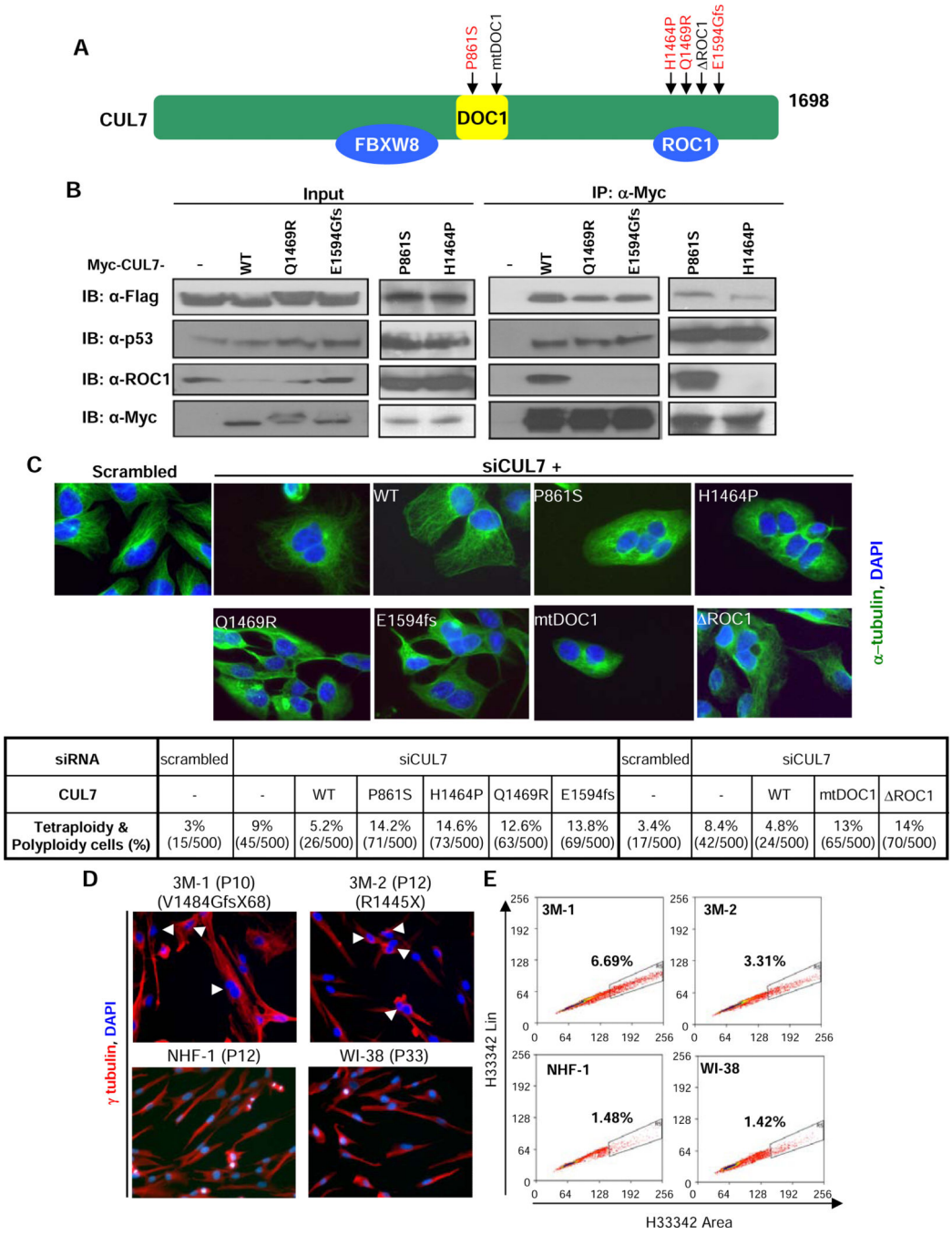

siRNA	scrambled	siCUL7						scrambled	siCUL7			
CUL7	-	-	WT	P861S	H1464P	Q1469R	E1594fs	-	-	WT	mtDOC1	ΔROC1
Tetraploidy & Polyploidy cells (%)	3% (15/500)	9% (45/500)	5.2% (26/500)	14.2% (71/500)	14.6% (73/500)	12.6% (63/500)	13.8% (69/500)	3.4% (17/500)	8.4% (42/500)	4.8% (24/500)	13% (65/500)	14% (70/500)

Figure 3. 3M derived mutations in CUL7 disrupt its function in regulating microtubule dynamics and maintaining genome integrity

(A) Schematic representation of human CUL7 protein. 3M patient derived mutations are indicated in red. The mutations targeting two functional domains, DOC1 and ROC1 binding, are also indicated.

(B) 293T cells were cotransfected with plasmids expressing indicated proteins. Two days after transfection, expression and association between CUL7 with FBXW8, p53 and ROC1 was determined by western or IP-western analyses.

(C) U2OS cells were transduced with retrovirus encoding siRNA resistant, Myc-tagged wild-type or various CUL7 mutants. Cells were then transfected with scrambled or CUL7 siRNA, followed by α-tubulin and DAPI staining. Images are representative views of each sample. Five hundred cells from each group were scored for polyploidy. See also Figure S3. (D, E) Normal human forehead fibroblasts NHF1, normal human lung fibroblasts WI38, and skin fibroblasts derived from two 3M patients bearing *CUL7* mutations were stained with α-tubulin (red) and DAPI (blue). Five hundred cells of each group were counted to score tetraploid cells (**D**), or stained with Hoechst 33342 and then subjected to FACS analysis to quantify polyploidy cells (**E**).

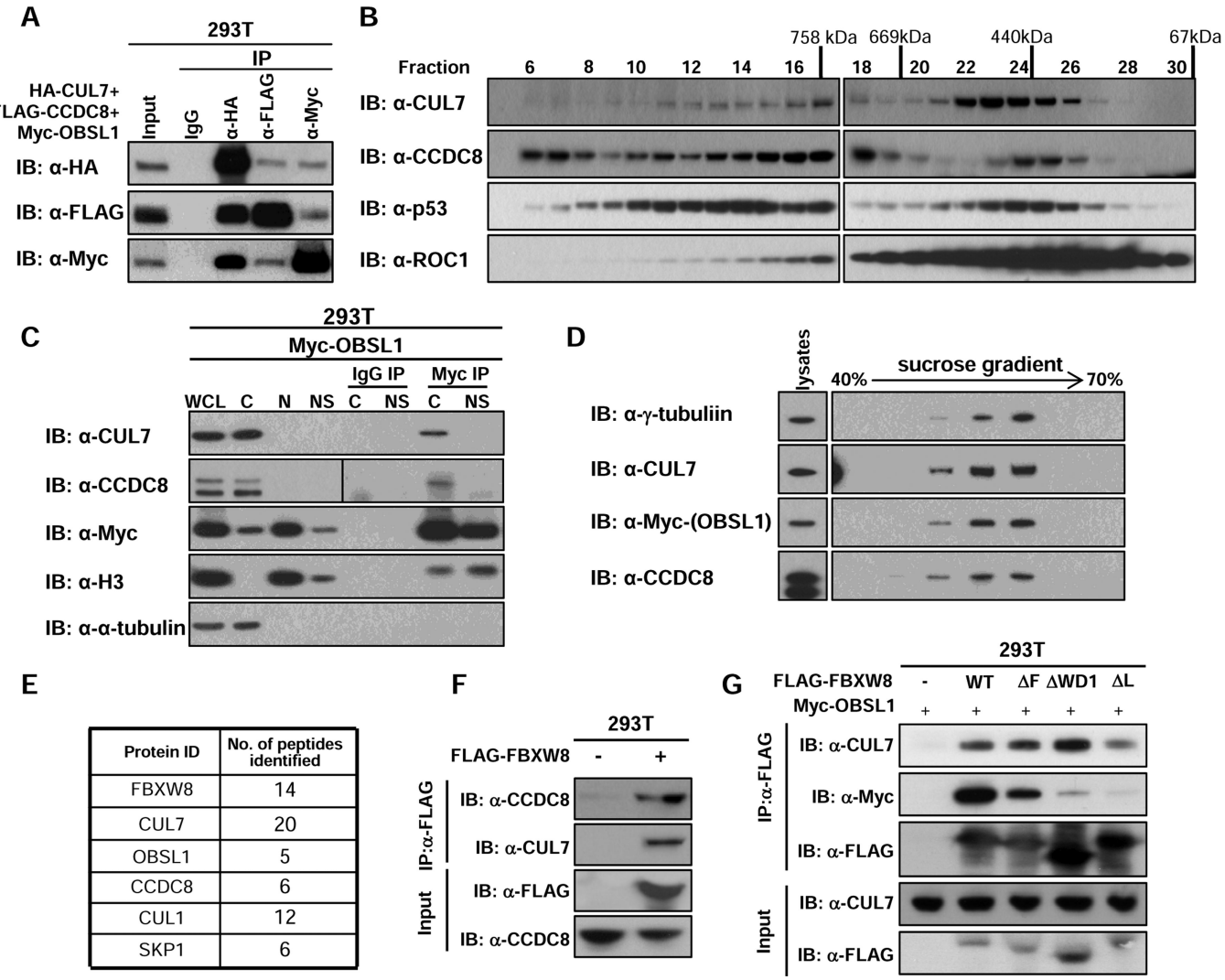

Protein ID	No. of peptides identified
FBXW8	14
CUL7	20
OBSL1	5
CCDC8	6
CUL1	12
SKP1	6

Figure 4. 3M proteins OBSL1 and CCDC8 interact with CUL7 and FBXW8 and form a large complex

(A) 293T cells were co-transfected with HA-CUL7, FLAG-CCDC8, and Myc-OBSL1. The association of the 3 proteins was tested by reciprocal IP/western assay. See also Figure S4A, B.

(B) Cell lysates from 293T cells were fractionated through gel filtration, and the indicated proteins were detected by western blot.

(C) 293T cells were overexpressed with Myc-OBSL1, and then the cytosolic (C), nuclear (N), and nuclear soluble (NS) fractions were prepared. Myc IP was performed in C and NS fractions, followed by western blot with the indicated antibodies.

(D) U2OS cells were transfected with Myc-OBSL1, and then the centrosomes were collected through a discontinuous sucrose gradient. The samples were subjected to western blot with the indicated antibodies.

(E) SBP-FBXW8 proteins complexes were purified and SBP-FBXW8 associated proteins were identified with mass spectrometry. Numbers of unique peptides identified are listed.

(F) FBXW8-CCDC8 interaction was detected by co-IP analysis in parental 293T and 293T cells stably expressing FLAG-FBXW8.

(G) Myc-OBSL1 was co-transfected with wild type FLAG-FBXW8 or its truncated mutants as indicated in 293T cells, and their interaction was detected by co-IP analysis.

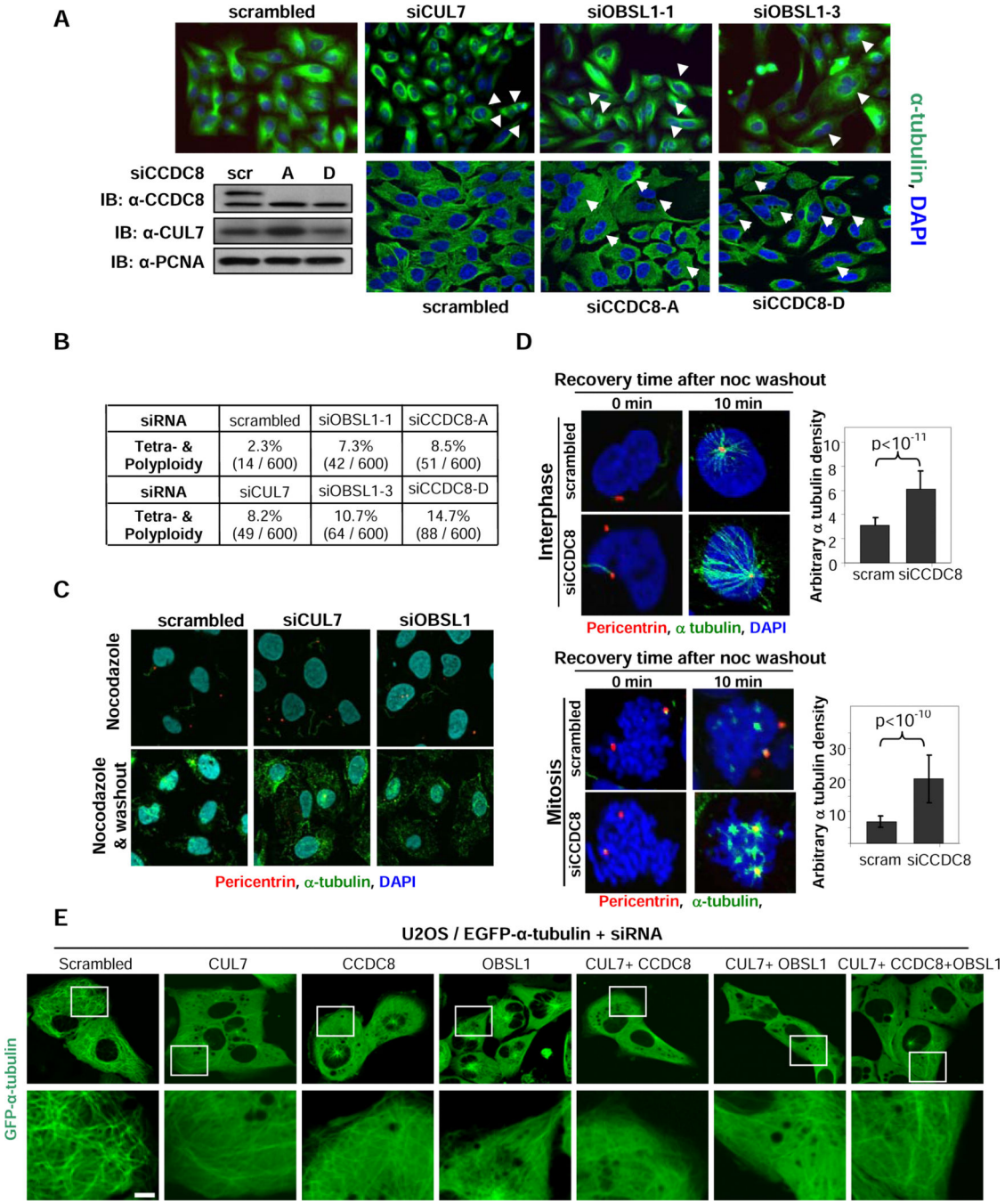

siRNA	scrambled	siOBSL1-1	siCCDC8-A
Tetra- & Polyploidy	2.3% (14 / 600)	7.3% (42 / 600)	8.5% (51 / 600)
siRNA	siCUL7	siOBSL1-3	siCCDC8-D
Tetra- & Polyploidy	8.2% (49 / 600)	10.7% (64 / 600)	14.7% (88 / 600)

Figure 5. 3M proteins OBSL1 and CCDC8 are required for maintaining microtubule and genome integrity

(A, B) U2OS cells were treated with scrambled, CUL7, two different OBSL1 and CCDC8 siRNA oligos, followed by α-tubulin and DAPI staining. Pictures are representative views of the samples. Arrowheads indicate tetraploidy or polyploidy cells (A). Tetraploid and polyploid cells of each sample were scored (B). See also Figure S5A

(C) U2OS cells were transfected with siCUL7 or siOBSL1. Seventy-two hours after transfection, cells were treated with 11μM nocodazole for two hours and then fixed at 0 and 10 min post-nocodazole washout and stained with the indicated antibodies.

(D) U2OS cells were transfected with siRNA against CCDC8 and then treated as described in (**C**). Representative interphase and mitotic cells were shown together with the statistics for the overall microtubule density. Error bars indicate standard deviation

(E) U2OS/EGFP-α-tubulin cells were transfected with the indicated siRNA oligos, and the microtubule network was observed with confocal microscopy. See also Figure S5B, C

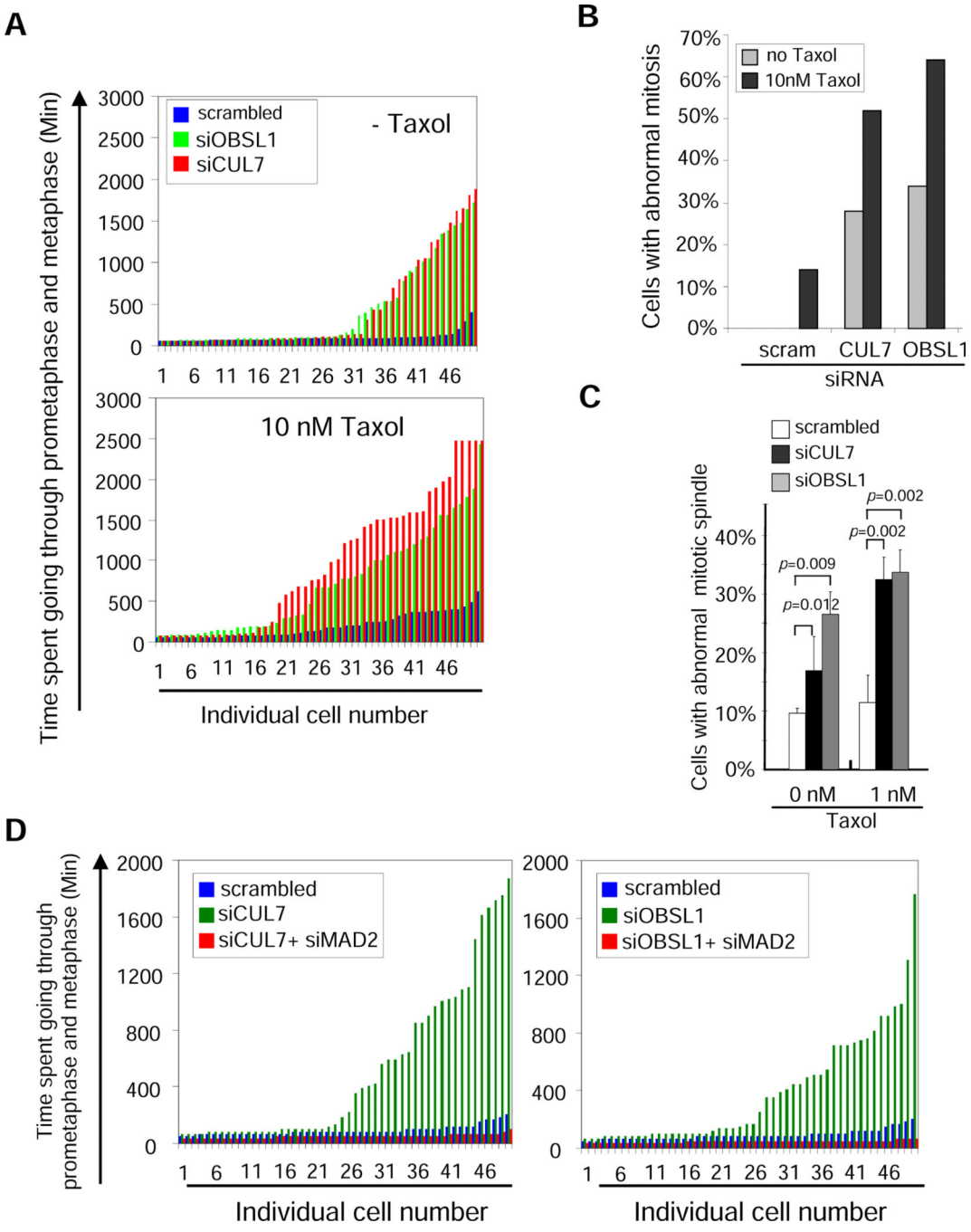

Figure 6. Loss of 3M genes function sensitizes cells to microtubule damage

(A, B) Human lung cancer cells NCI-H1155 stably expressing EGFP-Histone H2B were transfected with the indicated siRNA oligos for 48 hours. The cells were then either untreated or treated with 10 nM taxol for 24 hours, followed by imaging EGFP-Histone H2B every 14.5 minutes for 40 hours to trace mitosis. Duration from nuclear envelope break to anaphase was measured for 50 cells from each sample, and time intervals plotted (**A**). Cells exiting mitosis as dead cell, as a single cell, divided into more than 2 cells, or as multinucleated cells were scored as abnormal mitosis (B). See also Figure S6A

(C) U2OS/EGFP-α-tubulin cells were transfected with indicated siRNA oligo and then treated with or without 1nM taxol. Cells with either mono- or multi-polar mitotic spindles were scored as cells with abnormal mitotic spindle. Error bars indicate standard deviation (D) CUL7 and OBSL1 depletion induced mitotic defects are SAC dependent. NCI-H1155 stably expressing EGFP-Histone H2B was transfected with the indicated siRNA oligos for 48 hours. The cells were followed by imaging EGFP-Histone H2B every 14.5 minutes for 46 hours to trace mitosis. Duration from nuclear envelope break to anaphase was measured for 50 cells from each sample, and time intervals plotted. See also Figure S6B-D.

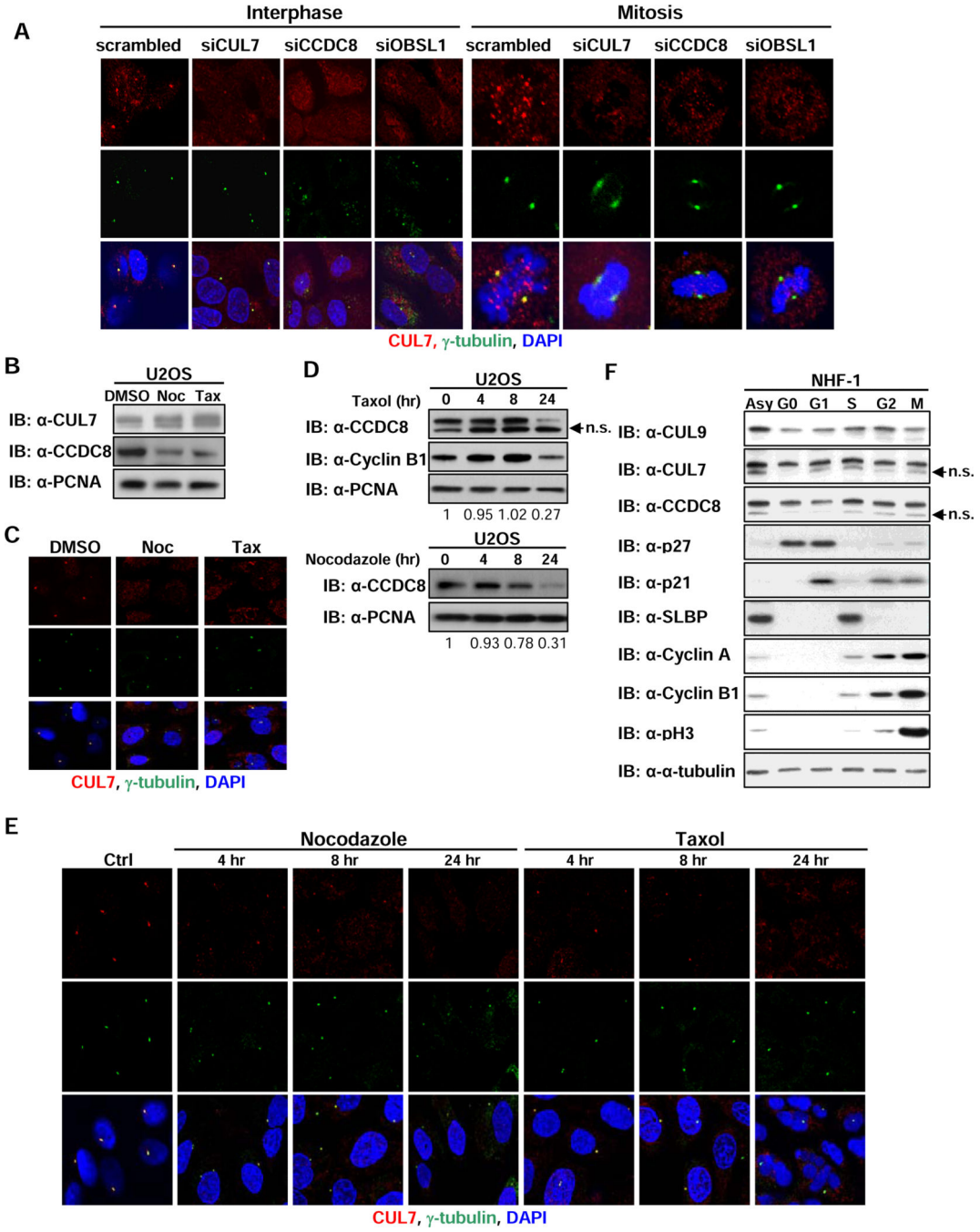

Figure 7. CCDC8 regulates CUL7 and is inhibited by microtubule damage

(A) U2OS depleted of CUL7, OBSL1, or CCDC8 were stained with the indicated antibodies, and representative images of the interphase and mitotic cells were shown. See also Figure S7B

(B) U2OS cells were treated with nocodazole (0.5μg/ml) or taxol (100 nM) for 24h, and the expression levels of the indicated proteins were determined by western blot.

(C) U2OS cells were treated as described in (B), and then were stained with the indicated antibodies. See also Figure S7C.

(D, E) U2OS cells were treated with nocodazole or taxol as indicated, and then CCDC8 protein levels (D) or CUL7 localization (E) was determined. See also Figure S7D.
(F) NHF-1 cells were synchronized into different phases, and then the indicated proteins were detected by western blot. See also Figure S7E, F.